ORIGINAL PAPER

Optimizing and control of effective synthesize parameters for Fe_3O_4 nanoparticles using response surface methodology

Muneer M. Ba-Abbad[1] · P. V. Chai[2] · Abdelbaki Benamour[1] · Dina Ewis[1] · Abdul Wahab Mohammad[3] · Ebrahim Mahmoudi[3]

Abstract

To control Fe_3O_4 nanoparticles (Fe_3O_4 NPs) size, different molar ratio of Fe^{2+} and Fe^{3+} as well as ammonium hydroxide (pH) was used to synthesize Fe_3O_4 NPs through co-precipitation method. The Box–Behnken design was selected to explore the interaction between process parameters (factors) such as Fe^{2+} molar ion, Fe^{3+} molar ion and pH on the final size. The interactive effect between the process variables was evaluated by analysis of variance (ANOVA). The quadratic model predicted by the Box–Behnken design was significant with a P value of < 0.0001. The optimum synthesis conditions were predicted by the model indicating optimum size obtained using 1.00 mol Fe^{2+} ion with 3.00 mol Fe^{3+} ion with pH at 12.00. From the experiment, the particle size was 10 ± 2 nm at optimum conditions, while the model predicted a particle size of 6.80 nm. The magnetic properties of Fe_3O_4 NPs were displayed typical ferromagnetic behavior with saturation magnetization value to be 49.729 emu/g. Finally, the optimized Fe_3O_4 NPs showed about 80% removal of Congo red (CR) dye, which confirms their applicability in adsorption process for future applications.

Keywords Fe_3O_4 nanoparticles · Coprecipitation method · Box–Behnken design · Analysis of variance

Introduction

Since the 1990s, magnetic Fe_3O_4 nanoparticles (Fe_3O_4 NPs) have emerged as an important material in biomedical and magnetic fields. In biomedical fields, Fe_3O_4 NPs have been used as drug carriers to enhance the magnetic resonance imaging MRI (Gupta et al. 2020; Khmara et al. 2019; Teymourian et al. 2013). The magnetic properties of Fe_3O_4 NPs enable their usage as a magnetic material in electronics as well as magnetic fluids such as ferrofluids, battery, catalysis and magnetic storage media (Nkutha et al. 2020; Wu and Huang 2017; Yao et al. 2015). Recently

Fe_3O_4 NPs have become one of the outstanding magnetic materials (as an adsorbent) in wastewater treatment applications. They can be used to treat wastewater contaminated by heavy metals such as Cadmium (II), Chromium (VI) and Copper (II) (Chen et al. 2017; Ewis et al. 2020; Hajizadeh et al. 2020; Matome et al. 2020). The advance in terms of combining nanotechnology and membrane technology has greatly expanded the use of Fe_3O_4 NPs by introducing them as nanofillers in membrane modification and concurrently enhancing the membrane application for wastewater treatment (Ba-Abbad et al. 2017; Daraei et al. 2013; Ewis et al. 2021). However, it is crucial to obtain high reactivity ultrafine Fe_3O_4 NPs with higher ratio of surface area to volume (Tang and Lo 2013). Therefore, techniques for preparing smaller and higher surface area to volume ratio of Fe_3O_4 nanoparticles are becoming more important. Various methods have been used to prepare Fe_3O_4 nanoparticles such as co-precipitation, polyol processes, thermal decomposition and micro-emulsion (Chen et al. 2011; Lu et al. 2013; Zhang et al. 2013). Among them, co-precipitation method has gained popularity because of its simplicity (Hariani et al. 2013), requirement of less expensive equipment and ability to consistently produce smaller Fe_3O_4 particles. During the

✉ Muneer M. Ba-Abbad
mbaabbad@qu.edu.qa

1 Gas Processing Centre, College of Engineering, Qatar University, P.O.Box 2713, Doha, Qatar

2 Department of Chemical and Petroleum Engineering, Faculty of Engineering, Technology and Built Environment, UCSI University, 56000 Cheras, Kuala Lumpur, Malaysia

3 Department of Chemical and Process Engineering, Faculty of Engineering and Built Environment, UniversitiKebangsaan Malaysia, 43600 Bangi, Selangor Darul Ehsan, Malaysia

co-precipitation method, the effect of process factors such as pH, Fe^{2+} to Fe^{3+} ion molar ratio as well as the interaction between process factors have to be considered in order to produce the desired Fe_3O_4 size for specific applications. The conventional technique for optimizing the process factors needs more and more experimental efforts, which consume more time- and yet ignore the interaction effects between the factors of the process. Such limitations may be overcome by a three-level statistical design as it can minimize the total number of experiments, provide appropriate models for process optimization and give better illustration of the inter-variable interactions. The most well-known statistical approach is response surface methodology (RSM), which consists of a central composite design (CCD) (Lingamdinne et al. 2020), Box–Behnken design (BBD) (Bahari et al. 2019) and D-optimal design (Ba-Abbad et al. 2013; Hariz et al. 2018). RSM has been proven to provide significantly improved results using few experimental runs.

Several studies applied RSM to control the size and properties of metal oxides nanoparticle during the preparation stage. In order to minimize the size and enhance the photocatalyst properties of ZnO nanoparticles, the D-optimal design as one of RSM designs is applied (Ba-Abbad et al. 2013). Three main factors have a significant influence on the particle size, which are molar ratio between starting materials (zinc acetate and oxalic acid), pH of the solution and the calcination temperature. The minimum size produced experimentally was 18 ± 2 nm compared to 22.9 nm which is predicted by the model (Ba-Abbad et al. 2013). Kuldeep Singh et al.(2020) prepared iron oxide nanoparticles using Coriandrum sativum L. Leaf extract (Singh et al. 2020). The study showed that volume of leaf extract, agitation speed, and temperature has a significant influence on the particle size. The developed model using Box–Behnken design produced smallest size of iron oxide nanoparticles (mean 161.5 nm) as the main target of applying the RSM and totally closed with predict under optimum condition (mean 157.3 nm). On the other hand, nickel oxide nanoparticle was synthesized and optimized through the sol–gel method using Box–Behnken design (Ba-Abbad et al. 2015). To control nickel oxide nanoparticle during synthesis to produce the smallest possible particle size, the molar ratio between starting materials (nickel nitrate and citric acid), pH of solution and calcination temperature were chosen as the most significant factors. Nickel oxide nanoparticles were synthesized under predicted condition by Box–Behnken design for the minimum particle size of 13.7 nm. The particle size produced experimentally as 14.3 nm was in a good agreement with the predicted size by Box–Behnken design.
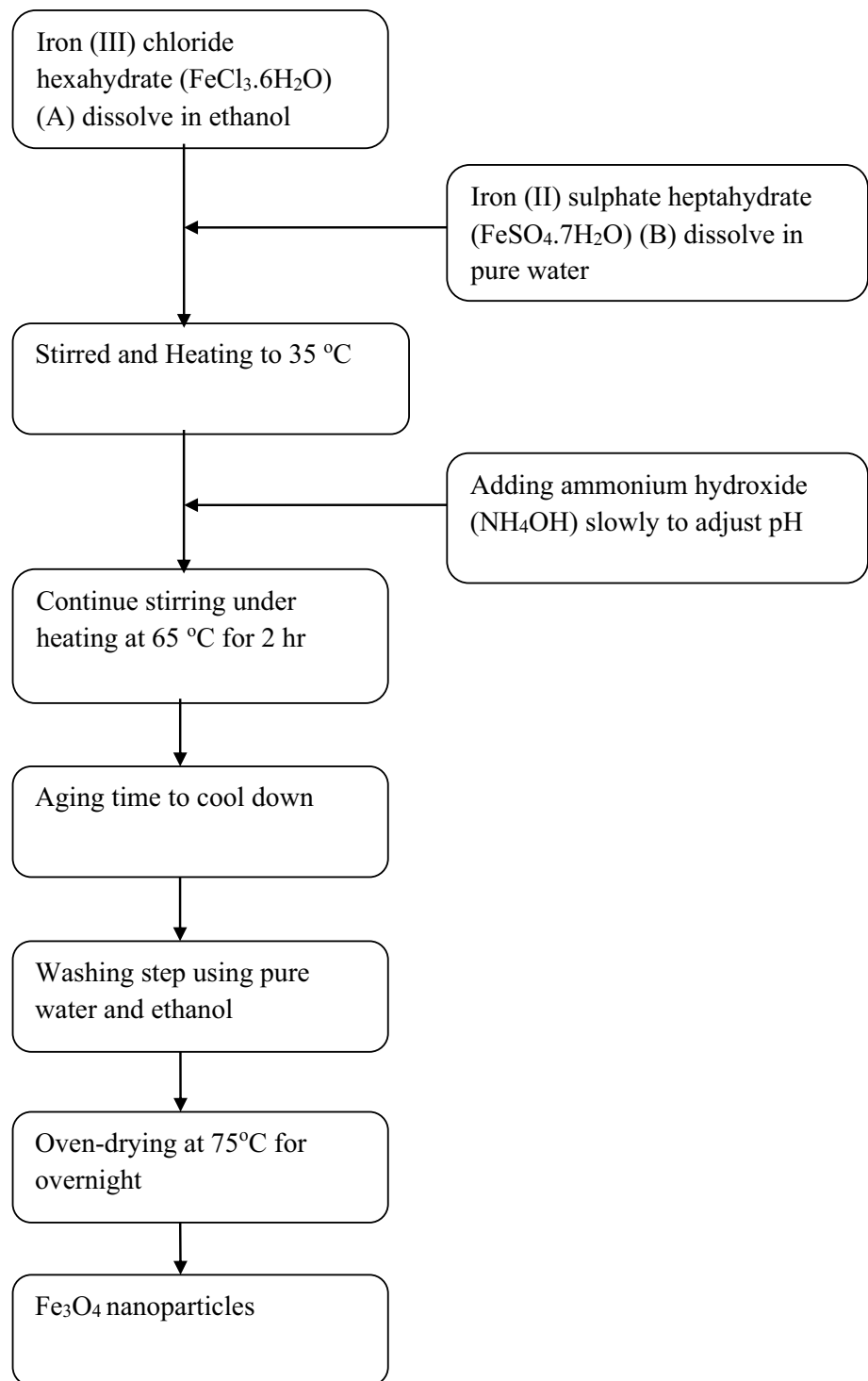
Therefore, the aim of this study is to produce the smallest size of Fe_3O_4 NPs using co-precipitation method without adding any additive such as capping agents or surfactants. To investigate this aim, the preparation conditions such

as molar ratio between Fe^{2+} and Fe^{3+} ions as well as pH were controlled, and the optimum process parameters were determined using Response Surface Methodology (RSM). These conditions of experiments were optimized using Box–Behnken design with particle size of Fe_3O_4 NPs as the response. Nevertheless, the literature shows no comprehensive optimization of these factors (Fe^{2+} and Fe^{3+} ions as well as pH) to produce the smallest possible size of Fe_3O_4 NPs. To the best of the authors' knowledge, there are no studies on optimizing the synthesis condition of Fe_3O_4 NPs using co-precipitation method with wide range of Fe^{2+} and Fe^{3+} ions molar ratio (1 to 3) and short range of pH (10–12). The previous study reported the ratio between Fe^{2+} and Fe^{3+} is 1:2, but ignored the effect of other ratios that can possibly produce smaller size of Fe_3O_4 NPs considering other factor such as pH. On the other hand, desired pH of solution was selected as factor in this study because to avoid any excess of ammonium hydroxide (ammonia) that used as volume (ml) in previous studies, which have been influenced on particle growth (Liu et al. 2022). This study shows complex interactions between factors that can be controlled to produce the minimum possible size of Fe_3O_4 NPs, which is not reported elsewhere. The results are expected to be the base for future studies aiming at developing Fe_3O_4 NPs using the co-precipitation method.

Materials and methods

Materials and methods

In order to synthesize Fe_3O_4 NPs, ferric chloride hexahydrate ($FeCl_3 \cdot 6H_2O$) which was supplied by Merck, Germany and ferrous sulfate heptahydrate ($FeSO_4 \cdot 7H_2O$) was ordered from Bendosen, Malaysia. The Ammonium hydroxide (NH_4OH) with 30% of ammonia in water was obtained from R&M Chemicals, Malaysia. Fe_3O_4 nanoparticles were synthesized by the co-precipitation method. Initially, $FeCl_3 \cdot 6H_2O$ and $FeSO_4 \cdot 7H_2O$ were dissolved in ethanol and pure water, respectively. After both solutions had completely dissolved, solution of $FeSO_4 \cdot 7H_2O$ was added slowly to the other solution of $FeCl_3 \cdot 6H_2O$. The final mixture was heated to 35 °C followed by the addition of NH_4OH to reach the desired pH. The solution mixture was stirred vigorously under heating at 60 °C for 2 h. The resulting solution was then left to cool followed by washing. Repeated washing was carried out using deionized water until the pH reached 7 ± 0.2 and the washing process was performed once with ethanol to remove remaining water. The final powder was kept overnight at 75 °C in an oven to remove remaining water and ethanol. Figure 1 shows the flow diagram of experimental procedures to synthesize Fe_3O_4 NPs.

Fig. 1 Flow diagram for Fe$_3$O$_4$ NPs synthesis

```
┌─────────────────────────┐
│ Iron (III) chloride      │
│ hexahydrate (FeCl₃.6H₂O) │
│ (A) dissolve in ethanol  │
└─────────────────────────┘
          │          ┌──────────────────────────────┐
          │◄─────────│ Iron (II) sulphate heptahydrate│
          │          │ (FeSO₄.7H₂O) (B) dissolve in   │
          │          │ pure water                     │
          ▼          └──────────────────────────────┘
┌─────────────────────────┐
│ Stirred and Heating to   │
│ 35 ºC                    │
└─────────────────────────┘
          │          ┌──────────────────────────────┐
          │◄─────────│ Adding ammonium hydroxide      │
          │          │ (NH₄OH) slowly to adjust pH    │
          ▼          └──────────────────────────────┘
┌─────────────────────────┐
│ Continue stirring under  │
│ heating at 65 ºC for 2 hr│
└─────────────────────────┘
          ▼
┌─────────────────────────┐
│ Aging time to cool down  │
└─────────────────────────┘
          ▼
┌─────────────────────────┐
│ Washing step using pure  │
│ water and ethanol        │
└─────────────────────────┘
          ▼
┌─────────────────────────┐
│ Oven-drying at 75ºC for  │
│ overnight                │
└─────────────────────────┘
          ▼
┌─────────────────────────┐
│ Fe₃O₄ nanoparticles      │
└─────────────────────────┘
```

The chemical reaction between the reactants to produce Fe$_3$O$_4$ NPs can be expressed by Eq. (1):

$$Fe^{2+} + 2Fe^{3+} + 8OH^- \xrightarrow{60°C} Fe_3O_4 + 4H_2O \tag{1}$$
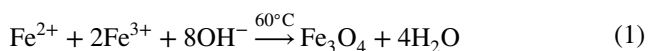
To test of Fe$_3$O$_4$ NPs performance for removal of Congo red (CR) dye as model of pollutant, the experiments were carried out in conical flask 50 ml. About 30 ml of CR solution with 20 ppm as initial concentration was shacked with certain dosage of Fe$_3$O$_4$ NPs as 0.05 and 0.1 g for 1 h at room temperature. After separation of Fe$_3$O$_4$ NPs using external magnet, final concentration of CR was measured

by UV–Vis spectrophotometer (Perkin Elmer, lambda 35). The removal (R %) of CR was calculated using Eq. (2):

$$R\% = \frac{C_0 - C}{C_0} \times 100 \tag{2}$$

where C_0 and C are the initial and final concentration of CR, which is determined by UV–Vis absorbance before and after adsorption process using Fe_3O_4 NPs.

Box–Behnken experimental design (BBD)

The statistical technique that uses a sequence of designed experiments to get optimal responses with given operating conditions is call response surface methodology. The BBD which is one of the RSM standard designs was selected to investigate the effect of the process factors according to the finally established empirical model. The BBD (Minitab 19) was selected in this study because of its ability to create designs with desirable statistical properties. BBD requires only a small number of experimental runs to determine the complex response function (Krishna and Padma Sree 2013). The derived complex response function can be fitted into a second-order polynomial model as shown in Eq. (3)

$$Y = C_0 + a = 1 \sum_{a=1}^{A} C_a x_a + \sum_{i=1}^{A} C_{aa} x_a^2 + \sum_{a=}^{A-1} \sum_{b=a+1}^{A} C_{ab} x_a x_b \tag{3}$$

where Y is the predicted response associated with each factor level combination, and C_0, C_a, C_{aa} and C_{ab} are the intercept term coefficient, linear term coefficient, quadratic term coefficient, and interaction coefficient, respectively. A x_a and x_b indicate the independent variables. Additionally, k is the number of the independent variables. In this study, three factors are considered which are Fe^{2+} ion molar ratio, Fe^{3+} ion molar ratio, pH, to determine their effect on the particle size as well as understand the interaction between them. The molar ratio of Fe^{2+} and Fe^{3+} ions was varied between 1 and 3 and the pH of the solution was ranged from 10 to 12 using ammonium hydroxide. The variations of the process parameters are summarized in Table 1. A combination of

Table 1 Process parameter used for Box–Behnken design

Independent variable parameters	Level		
	− 1	0	+ 1
Fe^{2+} (Molar Ratio)	1	2	3
Fe^{3+} (Molar Ratio)	1	2	3
pH	10	11	12

Table 2 Design layout of Box–Behnken and response for synthesized Fe_3O_4 NPs

Run No	Factor input variable			Response
	Fe^{2+} molar ratio	Fe^{3+} molar ratio	pH	Particle size (crystal size) nm
1	3	2	12	17.93
2	2	2	11	25.67
3	2	3	12	11.56
4	1	3	11	8.17
5	1	2	12	8.13
6	3	2	10	18.57
7	2	1	12	17.75
8	1	1	11	11.17
9	2	1	10	27.78
10	3	3	11	15.57
11	2	2	11	28.13
12	2	2	11	23.98
13	3	1	11	19.07
14	2	2	11	27.83
15	2	3	10	18.30
16	1	2	10	14.76
17	2	1	10	14.41

these process parameters was used to determine the response of the particle size, as given in Table 2. However, the BBD contained a total of experiments as (17) with (12) experiments organized in a factorial design at the midpoint of the edges of the process space and (5) replicate experiments at the center point to evaluate of experiments error (Gidwani and Vyas 2016).

Characterization

X-ray diffraction (XRD)

The crystal size and structure of synthesized Fe_3O_4 NPs were determined using XRD technique. The analysis was achieved using a diffraction meter (Bruker AXS D8 Advance, Germany). The Fe_3O_4 NPs samples were scanned of a 2θ angle from 55 to 80°. The Scherrer equation Eq. (4) was applied to calculate the crystal size average.

$$D = \frac{K\lambda}{\beta \cos\theta} \tag{4}$$

where β is the peak width at half-maximum (full width at half maximum (FWHM),), K is the constant of Scherer equation which $K = 0.89$, λ is X-ray wavelength which $\lambda = 1.5406$ Å and θ is the Bragg diffraction angle.

Morphology analysis using Transmission electron microscope (TEM)

The particle shape and size of synthesized Fe_3O_4 NPs were determined by a transmission electron microscope with model of JEOL, JEM-2010, Netherland. A small amount of Fe_3O_4 NPs was dispersed in ethanol using sonication. After that, one drop of the suspended solution was dropped on a carbon-coated grid with 400 mesh. After a certain time, the sample was dried and introduced to the TEM machine.

Results and discussion

Box–Behnken design model for Fe_3O_4 particle size

The effect of the independent variables such as molar ratio of Fe^{2+} to Fe^{3+} and pH on the response of Fe_3O_4 particle size were determined with a quadratic polynomial model created by analysis of variance (ANOVA) in Eq. (5).

$$
\begin{aligned}
Y = & -633.5 + 15.07(Fe^{2+}) + 51.92(Fe^{3+}) + 108.7(pH) \\
& - 6.920(Fe^{2+})^2 - 6.263(Fe^{3+})^2 - 4.910(pH)^2 \\
& - 0.125(Fe^{2+} * Fe^{3+}) + 1.497(Fe^{2+*}pH) \\
& - 2.520(Fe^{3+} * pH)
\end{aligned}
$$

(5)

where Y is the predicted particle size included all linear term, quadratic term, and interaction coefficients. This model can be applied to predict the particle size of Fe_3O_4. The developed Eq. (4) also shows that the main process parameter influencing the Fe_3O_4 particle size is the Fe^{2+} ion molar ratio followed by pH, as shown in Table 3.
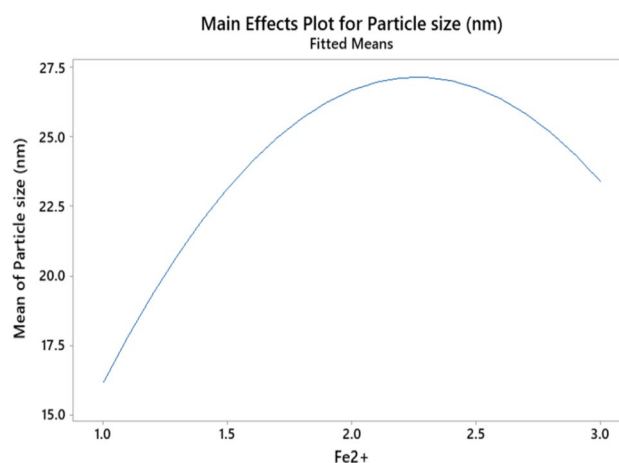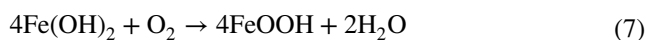

Fig. 2 Effects of Fe^{2+} ion molar ratio on Fe_3O_4 NPs size

Statistical model for Fe_3O_4 particle size analysis

Effect of Fe^{2+} ion molar ratio

Figure 2 illustrates the effect of Fe^{2+} ion molar ratio on Fe_3O_4 NPs size. The relationship between Fe^{2+} ion molar ratio and particle size appeared as a parabola shape in a second-order equation. Figure 2 shows that Fe_3O_4 particle size increases as the Fe^{2+} ion molar ratio increases from 1.0 to 2.5 and then decreases slightly when the molar ratio is more than 2.5. During the reaction, Fe^{2+} ion reacts with the OH^- to form $Fe(OH)_2$ by following Eq. (6). It is worth mentioning that as the amount of Fe^{2+} ion increases, more $Fe(OH)_2$ is generated. $Fe(OH)_2$ generated from Eq. (6) acts as an intermediate in Eq. (7), which reacts with O_2 to produce FeOOH and water. More $Fe(OH)_2$ and FeOOH compounds are produced at higher Fe^{2+} ion molar ratio, which

Table 3 ANOVA results for quadratic model of synthesized Fe_3O_4 NPs

Source	Sum of squares	Degree of freedom	Mean square	F-value	P value
Model	684.74	9	76.08	30.64	<0.0001
Fe^{2+}	104.47	1	104.47	42.08	0.0003
Fe^{3+}	9.68	1	9.68	3.90	0.0889
pH	14.23	1	14.23	5.73	0.0479
$(Fe^{2+})^2$	201.64	1	201.64	81.22	<0.0001
$(Fe^{3+})^2$	165.15	1	165.15	66.52	<0.0001
$(pH)^2$	101.52	1	101.52	40.89	0.0004
$(Fe^{2+}* Fe^{3+})$	0.063	1	0.063	0.025	0.8784
$(Fe^{2+*}pH)$	8.97	1	8.97	3.61	0.0991
$(Fe^{3+*}pH)$	25.40	1	25.40	10.23	0.0151
Residual	17.38	7	2.48	–	–
Lack of Fit	4.43	3	3.24	0.46	0.7271
Pure Error	12.95	4	–	–	–
Total	702.11	16	–	–	–

causes Fe_3O_4 particle size to increase accordingly (Coppola et al. 2016). As shown in Eq. (8), the reaction of $Fe(OH)_2$ with FeOOH ultimately produces Fe_3O_4 NPs. However, as the Fe^{2+} ion molar ratio increases to more than 2.5, Fe_3O_4 particle size starts to decrease. This was because the saturated condition has been reached (Yang et al. 2008).

$$Fe^{2+} + 2OH^- \rightarrow Fe(OH)_2 \tag{6}$$

$$4Fe(OH)_2 + O_2 \rightarrow 4FeOOH + 2H_2O \tag{7}$$

$$Fe(OH)_2 + 2FeOOH \rightarrow Fe_3O_4 + 2H_2O \tag{8}$$

Effect of pH

The effect of pH on the Fe_3O_4 NPs particle size also exhibited a quadratic shape of second-order relationship, as shown in Fig. 3. It can be observed that Fe_3O_4 particle size increased as the pH increased from 10 up to 11. Further increase in the pH has a divergent effect on Fe_3O_4 particle size reduction. However, within the reaction, the solution pH was adjusted using the NH_4OH which formed hydroxide (OH^-) ions and these ions reacted with Fe^{2+} and Fe^{3+} ions to form an intermediate compound of FeOOH. The amount of Fe^{2+} ion, Fe^{3+} ion and OH^-(adjusted by pH) in the reaction solution exhibited a great effect on the final size of the Fe_3O_4 NPs produced. As long as the amount of OH^- is sufficient, small Fe_3O_4 particle size is formed due to low concentration of $Fe(OH)_2$ and FeOOH (Eq. (8)), which caused control of particle growth. However, at pH 11 where the amount of OH^- was in excess and concentration of $Fe(OH)_2$ and FeOOH was higher, there was a fast formation of Fe_3O_4 particles. This growth eventually resulted in a bigger Fe_3O_4 particle size. The particle size decreased at pH more than 11
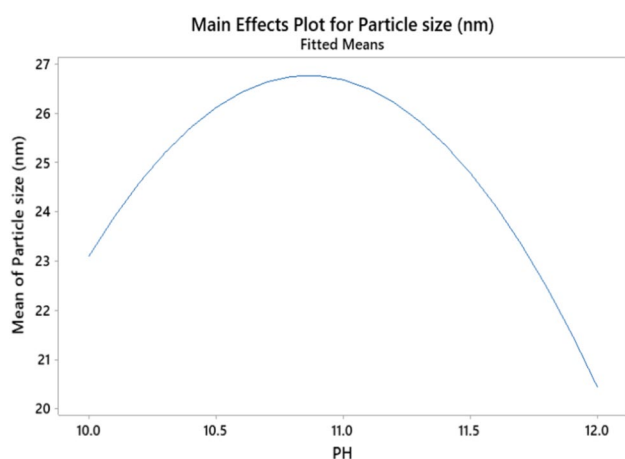
Fig. 3 Effects of pH on Fe_3O_4 NPs size

(More OH^- ions, available) because of the rapid formation of ferric hydroxide, as in Eq. (9 and 10) as follows (Suppiah and Abd Hamid 2016).

$$Fe^{3+} + 3OH^- \rightarrow Fe(OH)_3 \tag{9}$$

$$Fe(OH)_2 + 2Fe(OH)_3 \rightarrow Fe_3O_4 + 4H_2O \tag{10}$$
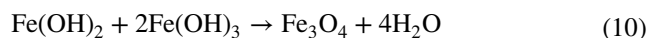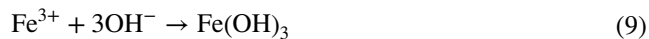
Response surface diagram and optimization

The statistical analysis of variance (ANOVA) is essential to investigate the significance of the predicted model. Table 3 shows all levels of Fe^{2+} ion molar ratio and pH are significant since the P value < 0.0001. The parameter is statistically significant when the P value < 0.05. The 'lack of Fit is 0.46 which implies that the parameter itself is not significant. Contour diagrams of interaction between process parameters that show the effect on Fe_3O_4 nanoparticle size response are given in Fig. 4. These diagrams can be used to recognize the effect of these factors on Fe_3O_4 particle size. Figure 4(A1 and A2) shows the interaction between Fe^{2+} and Fe^{3+} ion molar ratios on Fe_3O_4 particle size. From this interaction, the contour diagrams suggest that 1.00 mol of Fe^{2+} ion molar ratio should be used with 3.00 mol of Fe^{3+} ion molar ratio to produce minimal Fe_3O_4 particle size. The effect of Fe^{2+} ion molar ratio and pH on Fe_3O_4 nanoparticle size response are shown in Fig. 4(B1 and B2). The interaction effect of Fe^{2+} ion molar ratio and pH also showed a quadratic relation to the response of Fe_3O_4 particle size. The size increases as the pH of solution is more than 10.0 (with constant of Fe^{2+} ion) and then decreases observing the smallest size at pH 12. This is attributed to excess OH^- ions that promotes the production of $Fe(OH)_2$ and FeOOH (Eq. (7)) and fasten the formation of Fe_3O_4 particles. At the same time, a similar effect was observed on the Fe_3O_4 particle size as the Fe^{2+} ion (with constant pH) ratio increased more than 1.0 followed by particle size reduction when the ratio of Fe^{2+} ion is more than 1.0. The interaction between Fe^{2+} ion molar ratio and pH have the strongest effects on Fe_3O_4 particle size. These factors also showed the most significant effects on Fe_3O_4 particle size based on the p value obtained from ANOVA analysis. Figure 4(C1 and C2) indicates the effect of Fe^{3+} ion molar ratio and pH of the medium on Fe_3O_4 nanoparticle size. These factors have less effect on particle size when they were working together than Fe^{2+} ion molar ratio and pH in Fig. 4(B1, B2). A similar pattern in particle size is observed when pH value ranged from 10 to 12 and Fe^{3+} ion molar ratio ranged from one to three. This phenomenon was also observed in other works which confirmed a weaker influence of Fe^{3+} ion molar ratio on the size of Fe_3O_4 (Chen et al. 2010; Rajput et al. 2016).
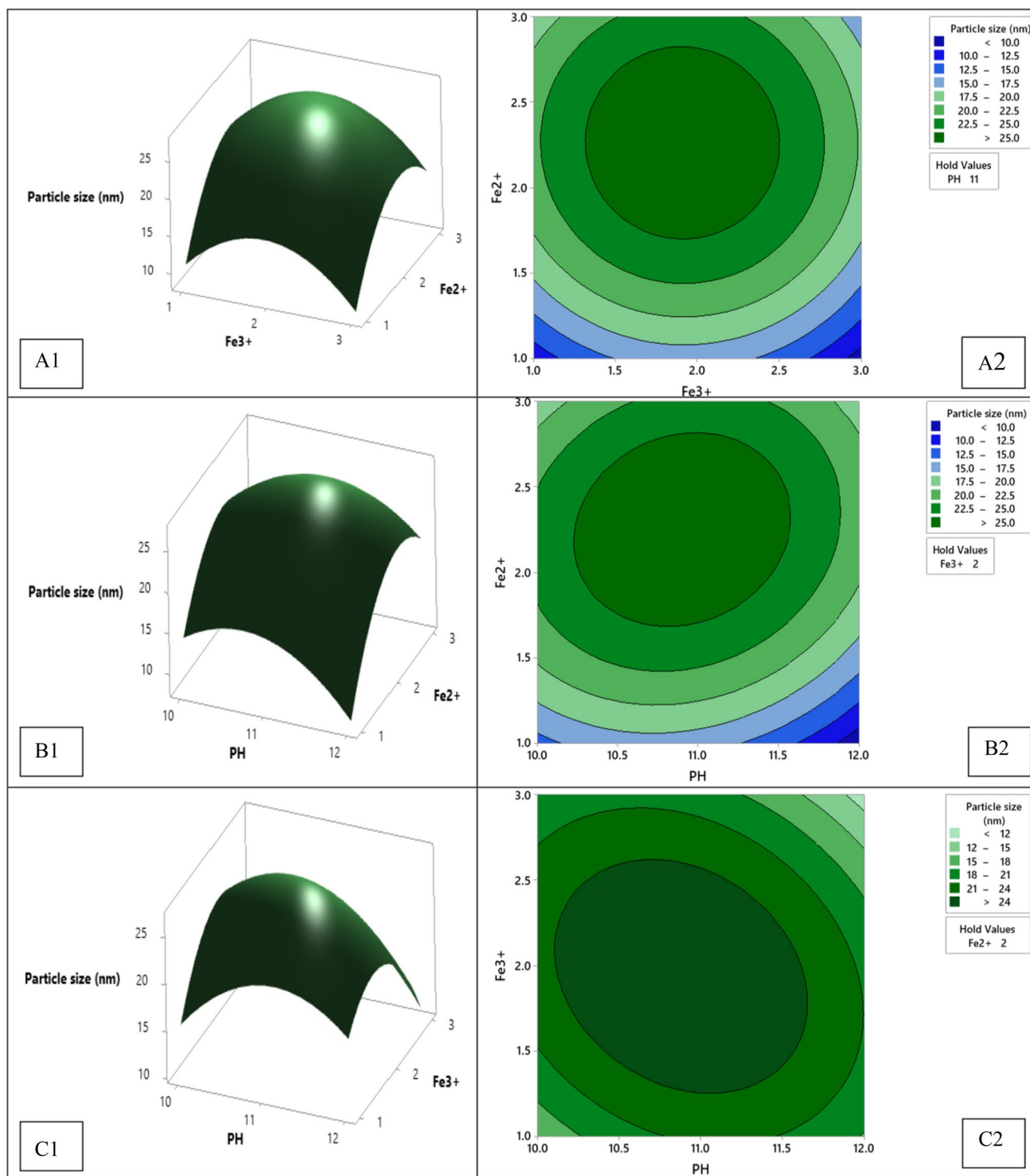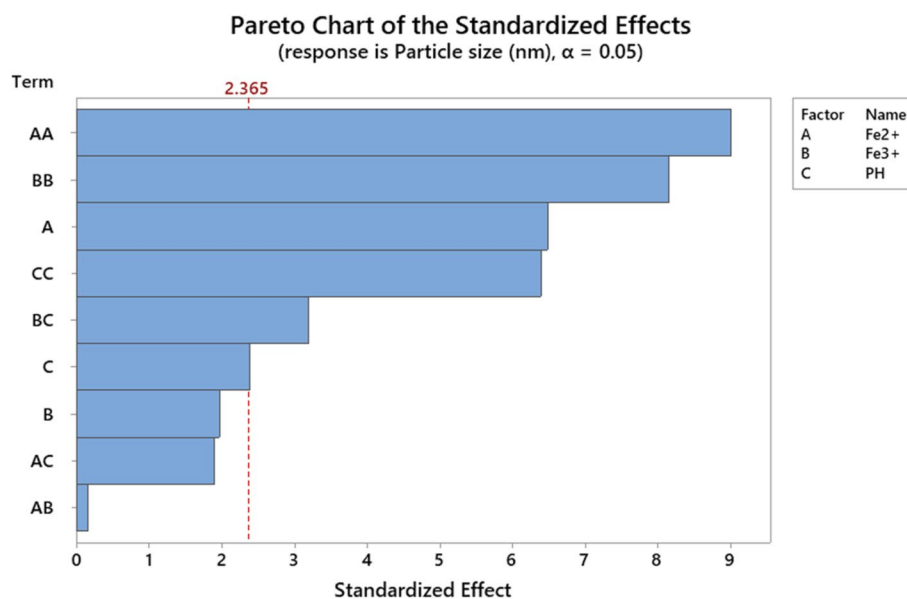
Fig. 4 Interactions between (A1, A2) Fe^{2+} ion to Fe^{3+} ion molar ratio, (B1, B2) Fe^{2+} ion molar ratio and pH, (C1, C2) Fe^{3+} ion molar ratio and pH on Fe_3O_4 NPs size

Pareto Chart of the Standardized Effects
(response is Particle size (nm), α = 0.05)

Pareto chart for the ANOVA table is given in Fig. 5 and important to show each independent variables with their effects as percentage on the response. The most effects factors from chart are Fe^{2+} ion molar ratio and pH, which are listed in their higher order of significance to control of Fe_3O_4 NPs size. These results showed in good agreement with analysis data from RSM diagrams and ANOVA table.

Model regression verification

The empirical model of Fe_3O_4 particle size which indicates the validity and the reliability of the model as the value of R-squared (0.9752) and Adj R-squared (0.9736), are relatively high. Figure 6a shows the plot of the normality % probability versus studentized residuals, which confirms that errors are under normal distribution. As can be seen from Fig. 6a, the tabulation of the residuals are close to the straight line, which confirms that the distribution is normal. If the tabulation of residuals is far from the straight line, the error will be significant and this will affect the significance of the predicted model. Figure 6b shows the balanced scattering of points above and below the x-axis in which no unusual structure was observed. Figure 6c shows the plot of predicted versus actual value of Fe_3O_4 particle size. These results confirmed the higher adequacy of the model with the correlation coefficient, R^2. At the same time, the empirical model showed that experimental results are in a good fit with model. ANOVA analyses suggest that the model derived by

the Box–Behnken design is reliable in terms of predicting the Fe_3O_4 NPs size.

To achieve the optimum condition for Fe_3O_4 minimal size, four optimization criteria are required, (as minimum, maximum, within the range and target) and the values of these criteria were applied as shown in Table 4.

Accordingly, the model equation predicted that the minimal size of particles is 6.80 nm, which is produced by 1.00 molar ratio of Fe^{2+} ion and 3.00 molar ratio of Fe^{3+} ion with pH at 12.00, as given in Fig. 7. These results are in a good agreement with the interpretation of the contour diagram. To verify the validity of the result, experiments were carried out with three replicates to prepare Fe_3O_4 nanoparticles in optimal conditions. The average result obtained from the XRD was 10 ± 3 nm and that from TEM was 10 ± 2 nm. This confirmed the effectiveness and reliability of the predicted values from the prediction model.

Characterization of Fe_3O_4 nanoparticles

The average particle size of the Fe_3O_4 NPs for three replicates was evaluated by XRD analysis. The size of Fe_3O_4 determined by XRD analysis was found to be 10 ± 3 nm. Figure 8 shows the XRD diagram for the Fe_3O_4 NPs using optimal condition as 1.00 molar ratio of Fe^{2+} ion and 3.00 molar ratio of Fe^{3+} ion with pH at 12.00. All peak positions of Fe_3O_4 matched at 2θ of 30.21°, 35.72°, 43.34°, 53.35°,
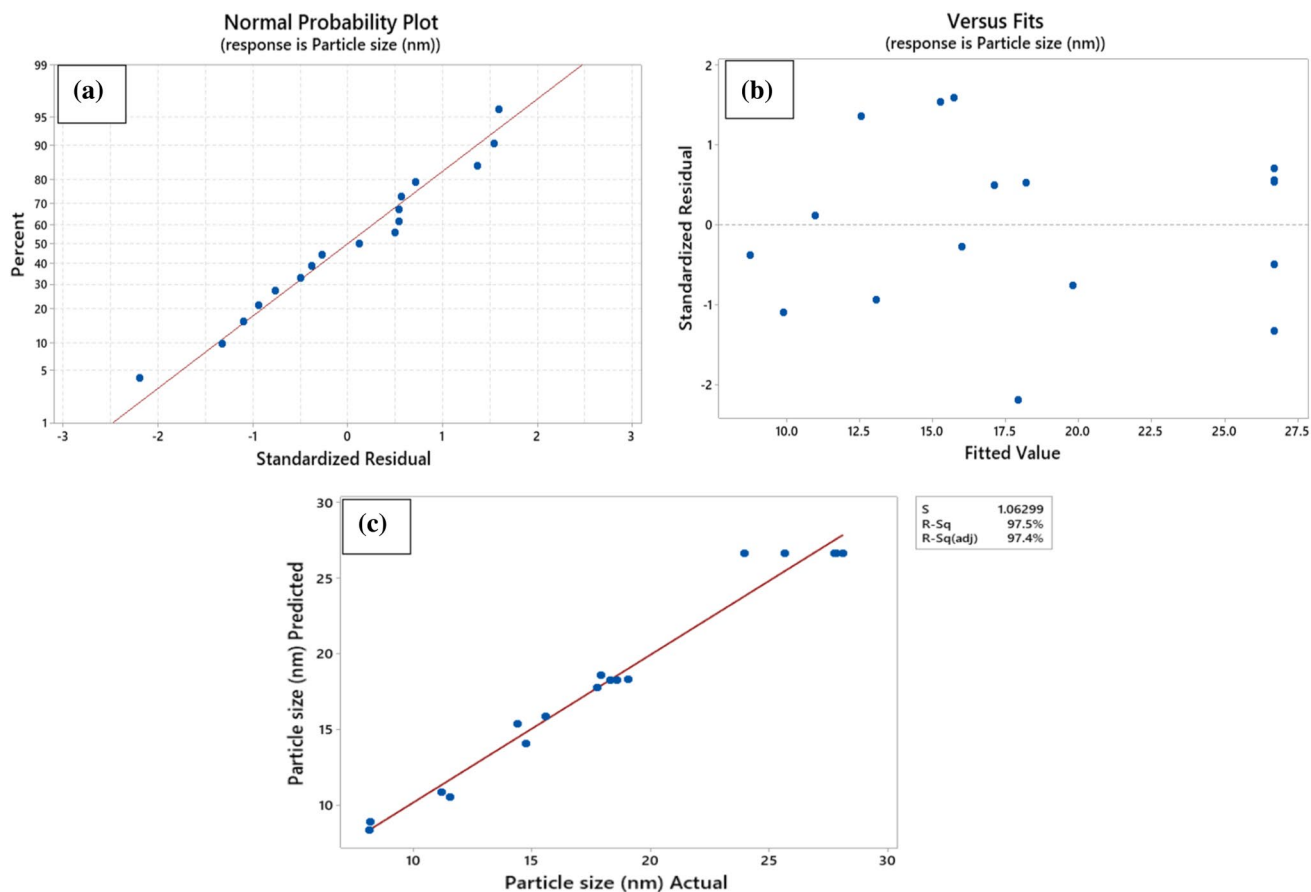
Fig. 6 Diagnostic plots of Fe_3O_4 synthesis **a** normal % probability versus studentized residuals, **b** studentized residuals versus predicted, **c** predicted plot versus actual

Table 4 Optimization of all factors to obtain minimum size for Fe_3O_4 NPs

Process parameter	Goal	Lower limit	Upper limit
Fe^{2+} (Molar Ratio)	Is in range	1	3
Fe^{3+} (Molar Ratio)	Is in range	1	3
pH	Is in range	10	12
Particle Size (nm)	minimum	8.13	28.13

57.37° and 63.07° were found. The position of peaks shows exactly for data of diffraction face-centered cubic (FCC) crystalline as reported in previous studies (Petcharoen and Sirivat 2012; Valenzuela et al. 2009).

The TEM analysis was carried out to support XRD analysis results. The TEM image of Fe_3O_4 NPs which was prepared under optimal conditions showed almost spherical shapes with an average of 10 ± 2 nm, as given in Fig. 9.

Fig. 7 The optimum conditions predicted by the Box–Behnken design for minimal size of Fe_3O_4 NPs
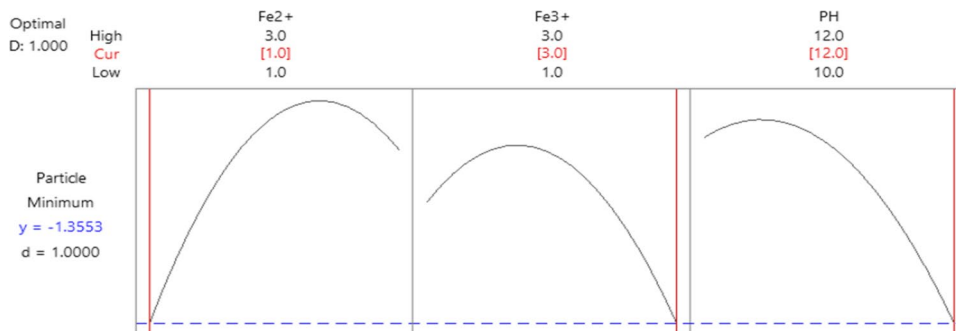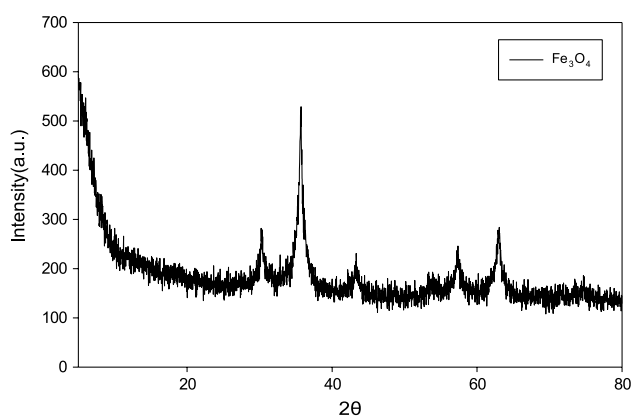
Fig. 8 X-ray patterns of Fe$_3$O$_4$ NPs prepared under optimum conditions
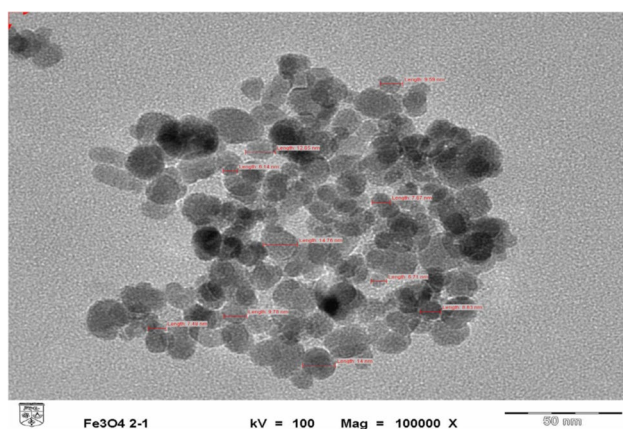
Fig. 9 Transmission electron microscope (TEM) of Fe$_3$O$_4$ NPs prepared under optimum conditions
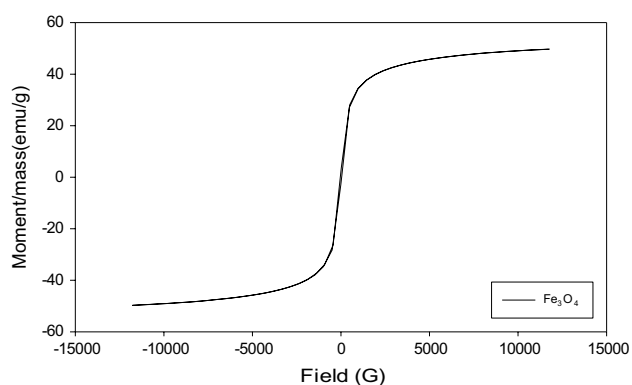

Fig. 10 Room-temperature magnetic hysteresis loops for Fe$_3$O$_4$ NPs prepared under optimum conditions

These results are in a good agreement with the result from the XRD analysis. The agglomeration of Fe$_3$O$_4$ NPs was mainly contributed by the drying procedure during preparation of TEM samples.

Figure 10 shows the M–H curve measurements of the Fe$_3$O$_4$ NPs prepared under optimum conditions, which saturation magnetization value was found to be 49.729 emu/g. The magnetic properties of Fe$_3$O$_4$ NPs displayed typical ferromagnetic behavior and were close to those reported elsewhere (Beyaz et al. 2009; Rahdar and Arabi 2012).

The adsorption test on Congo red (CR) removal was done to study the applicability of the synthesized of Fe$_3$O$_4$ NPs. Tests were carried out using the optimal synthesis condition of Fe$_3$O$_4$ NPs only. Two sets of experiments were conducted to determine effect of the certain amount of Fe$_3$O$_4$ NPs from 0.05 to 0.1 g on CR removal efficiency. However, higher removal of CR was achieved as 82.34% using 0.1 g compare 58.79% by 0.05 g under the same experimental conditions. Furthermore, as shown in Fig. 11, Fe$_3$O$_4$ NPs can be easily separated by a magnetic field from the CR aqueous solution. In general, the co-precipitation method in this study managed to produce smaller Fe$_3$O$_4$ NPs because of its high flexibility compared with the other synthesis methods, producing nanoparticles with various properties. In terms of ease of operation, this method was simple and produced consistently small Fe$_3$O$_4$ NPs in the range of 10 nm. This method does not require the usage of any capping agent or surfactant (or any other additives) and thus reduces the cost of chemicals. Furthermore, this method does not require the use of high temperature and pressure and specialized equipment. This study showed an improved BBD optimization to produce of smaller Fe$_3$O$_4$ NPs sizes and control effects of the process parameters and their interaction during preparation stage. The bigger Fe$_3$O$_4$ NPs obtained with the co-precipitation method can be endorsed to their lack conditions out of predicted optimal conditions for selected variables within the preparation process (Hou et al. 2014).

Conclusions

Fe$_3$O$_4$ nanoparticles were successfully optimized via a Box–Behnken design. The effects of process parameters (factors) and their interactions on the Fe$_3$O$_4$ NPs size response were investigated by ANOVA analysis. The design showed that Fe^{2+} ion molar ratio and pH had the

Fig. 11 Adsorption of Congo red using different amount of Fe_3O_4 NPs **a** 0.0 g **b** 0.05 g **c** 0.10 g

(a) 0.0g **(b)** 0.05g **(c)** 0.10g
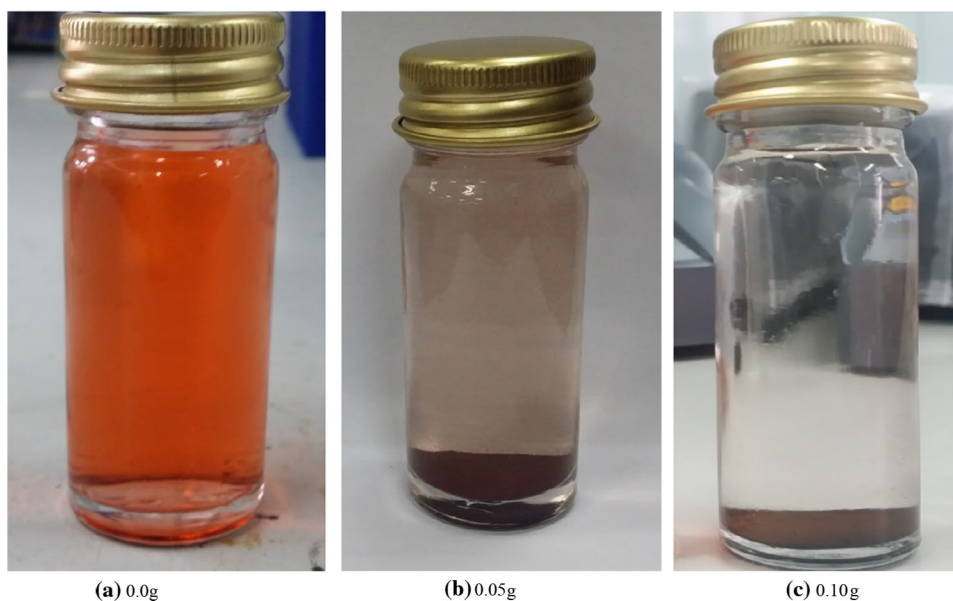
highest effect on the response (particle size). The empirical model shows good validity and reliability as the R-squared (0.9752) and Adj R-squared (0.9736) are relatively high. The optimal conditions determined by the empirical model for minimal Fe_3O_4 NPs size were observed at 1.00 mol Fe^{2+} ion with 3.00 mol Fe^{3+} ion with pH at 12.00. The predicted particle size of Fe_3O_4 was 6.80 nm and the experimental values were found to be 10 ± 3 nm and 10 ± 2 nm, as evaluated by XRD and TEM analysis, respectively. Fe_3O_4 particle size from experimental and theoretical values shows that the predicted empirical model is reliable, and could be utilized as a suitable optimization model. Finally, the optimized Fe_3O_4 NPs showed about 80% removal of Congo red (CR) dye, which confirms their applicability in adsorption process for future applications.

Declarations

Conflict of interest On behalf of all authors, the corresponding author states there is no conflict of interest.

Human and animal participants This article does not contain any studies with human participants or animals performed by any of the authors.

References

Ba-Abbad MM, Kadhum AAH, Mohamad AB, Takriff MS, Sopian K (2013) Optimization of process parameters using D-optimal design for synthesis of ZnO nanoparticles via sol–gel technique. J Ind Eng Chem 19:99–105

Ba-Abbad MM, Chai PV, Takriff MS, Benamor A, Mohammad AW (2015) Optimization of nickel oxide nanoparticle synthesis through the sol–gel method using Box-Behnken design. Mater Des 86:948–956

Ba-Abbad MM, Mohammad A, Takriff MS, Rohani R, Mahmoudi E, Faneer K, Benamor A (2017) Synthesis of iron oxide nanoparticles to enhance polysulfone ultrafiltration membrane performance for salt rejection. Chem Eng Trans 56:1699–1704

Bahari NA, Isahak WNRW, Masdar MS, Ba-Abbad MM (2019) Optimization of the controllable crystal size of iron/zeolite nanocomposites using a Box-Behnken design and their catalytic activity. Appl Nanosci 9:209–224

Beyaz S, Köçkar H, Tanrisever T (2009) Simple synthesis of superparamagnetic magnetite nanoparticles and ion effect on magnetic fluids. J Optoelec Adv Mater-Symp 1:447–450

Chen L, Zhao C, Zhou Y, Peng H, Zheng Y (2010) Controlled synthesis of Fe_3O_4 nanosheets via one-step pyrolysis of EDTA ferric sodium salt. J Alloys Compd 504:L46–L50

Chen L, Lin Z, Zhao C, Zheng Y, Zhou Y, Peng H (2011) Direct synthesis and characterization of mesoporous Fe_3O_4 through pyrolysis of ferric nitrate-ethylene glycol gel. J Alloys Compd 509:L1–L5

Chen S, Zhou R, Chen Y, Fu Y, Li P, Song Y, Wang L (2017) Carbon-covered Fe_3O_4 hollow cubic hierarchical porous composite as the anode material for lithium-ion batteries. J Nanopart Res 19:127–140

Coppola P, da Silva FG, Gomide G, Paula FL, Campos AFC, Perzynski R, Kern C, Depeyrot J, Aquino R (2016) Hydrothermal synthesis of mixed zinc–cobalt ferrite nanoparticles: structural and magnetic properties. J Nanopart Res 18:138–153

Daraei P, Madaeni SS, Ghaemi N, Khadivi MA, Astinchap B, Moradian R (2013) Fouling resistant mixed matrix polyethersulfone membranes blended with magnetic nanoparticles: Study of magnetic field induced casting. Sep Purif Technol 109:111–121

Ewis D, Benamor A, Ba-Abbad MM, Nasser M, El-Naas M, Qiblawey H (2020) Removal of oil content from oil-water emulsions using iron oxide/bentonite nano adsorbents. J Water Process Eng 38:101583–101593

Ewis D, Ismail NA, Hafiz M, Benamor A, Hawari AH (2021) Nanoparticles functionalized ceramic membranes: fabrication, surface modification, and performance. Environ Sci Pollut Res 28:12256–12281

Gidwani B, Vyas A (2016) Preparation, characterization, and optimization of altretamine-loaded solid lipid nanoparticles using Box-Behnken design and response surface methodology. Artif Cells Nanomed Biotechnol 44:571–580

Gupta PK, Dravid VP, De M (2020) ultrathin silica-coated iron oxide nanoparticles: size-property correlation. ChemistrySelect 5:8929–8934

Hajizadeh Z, Valadi K, Taheri-Ledari R, Maleki A (2020) Convenient Cr(VI) removal from aqueous samples: executed by a promising clay-based catalytic system, magnetized by Fe_3O_4 nanoparticles and functionalized with humic acid. ChemistrySelect 5:2441–2448

Hariani P, Faizal M, Syarofi R, Marsi M, Setiabudidaya D (2013) Synthesis and properties of Fe_3O_4 nanoparticles by co-precipitation method to removal procion dye. Int J Environmental Sci Dev 4:336–340

Hariz HB, Takriff MS, Ba-Abbad MM, Mohd Yasin NH, Mohd Hakim NIN (2018) CO_2 fixation capability of Chlorella sp. and its use in treating agricultural wastewater. J Appl Phycol 30:3017–3027

Hou L, Zhang Q, Jérôme F, Duprez D, Zhang H, Royer S (2014) Shape-controlled nanostructured magnetite-type materials as highly efficient Fenton catalysts. Appl Catal B 144:739–749

Khmara I, Strbak O, Zavisova V, Koneracka M, Kubovcikova M, Antal I, Kavecansky V, Lucanska D, Dobrota D, Kopcansky P (2019) Chitosan-stabilized iron oxide nanoparticles for magnetic resonance imaging. J Magn Magn Mater 474:319–325

Krishna D, Padma Sree R (2013) Response surface modeling and optimization of chromium (VI) removal from aqueous solution using borasus flabellifer coir powder (2013). Int J Appl Sci 11:213–226

Lingamdinne LP, Choi JS, Choi YL, Chang YY, Yang JK, Karri RR, Koduru JR (2020) Process modeling and optimization of an iron oxide immobilized graphene oxide gadolinium nanocomposite for arsenic adsorption. J Mol Liq 299:112261

Liu D, Huang L, Li T, Zhang G, Ni Q (2022) Cucurbit[6]uril-functionalized Fe3O4 magnetic nanoparticles for pH-responsive drug delivery. Chem Pap 76:3853–3862

Lu T, Wang J, Yin J, Wang A, Wang X, Zhang T (2013) Surfactant effects on the microstructures of Fe_3O_4 nanoparticles synthesized by microemulsion method. Colloids Surf a: Physicochem Eng Asp 436:675–683

Matome SM, Makhado E, Katata-Seru LM, Maponya TC, Modibane KD, Hato MJ, Bahadur I (2020) Green synthesis of polypyrrole/nanoscale zero valent iron nanocomposite and use as an adsorbent for hexavalent chromium from aqueous solution. S Afri J Chem Eng 34:1–10

Nkutha CS, Shooto ND, Naidoo EB (2020) Adsorption studies of methylene blue and lead ions from aqueous solution by using mesoporous coral limestones. S Afri J Chem Eng 34:151–157

Petcharoen K, Sirivat A (2012) Synthesis and characterization of magnetite nanoparticles via the chemical co-precipitation method. Mater Sci Eng B 177:421–427

Rahdar A, Arabi H (2012) Preparation of super paramagnetic iron oxide nanoparticles and investigation their magnetic properties. Int J Sci Eng Invest 1:10312–10313

Rajput S, Pittman CU, Mohan D (2016) Magnetic magnetite (Fe_3O_4) nanoparticle synthesis and applications for lead (Pb^{2+}) and chromium (Cr^{6+}) removal from water. J Colloid Interface Sci 468:334–346

Singh K, Chopra DS, Singh D, Singh N (2020) Optimization and eco-friendly synthesis of iron oxide nanoparticles as potential antioxidant. Arab J Chem 13:9034–9046

Suppiah DD, Abd Hamid SB (2016) One step facile synthesis of ferromagnetic magnetite nanoparticles. J Magn Magn Mater 414:204–208

Tang SCN, Lo IMC (2013) Magnetic nanoparticles: Essential factors for sustainable environmental applications. Water Res 47:2613–2632

Teymourian H, Salimi A, Khezrian S (2013) Fe_3O_4 magnetic nanoparticles/reduced graphene oxide nanosheets as a novel electrochemical and bioelectrochemical sensing platform. Biosens Bioelectron 49:1–8

Valenzuela R, Fuentes MC, Parra C, Baeza J, Duran N, Sharma SK, Knobel M, Freer J (2009) Influence of stirring velocity on the synthesis of magnetite nanoparticles (Fe_3O_4) by the co-precipitation method. J Alloys Compd 488:227–231

Wu M, Huang S (2017) Magnetic nanoparticles in cancer diagnosis, drug delivery and treatment. Mol Clin Oncol 7:738–746

Yang TI, Brown RNC, Kempel LC, Kofinas P (2008) Magneto-dielectric properties of polymer–Fe_3O_4 nanocomposites. J Magn Magn Mater 320:2714–2720

Yao X, Sabyrov K, Klein T, Lee Penn R, Wiedmann TS (2015) Evaluation of magnetic heating of asymmetric magnetite particles. J Magn Magn Mater 381:21–27

Zhang B, Tu Z, Zhao F, Wang J (2013) Superparamagnetic iron oxide nanoparticles prepared by using an improved polyol method. Appl Surf Sci 266:375–379